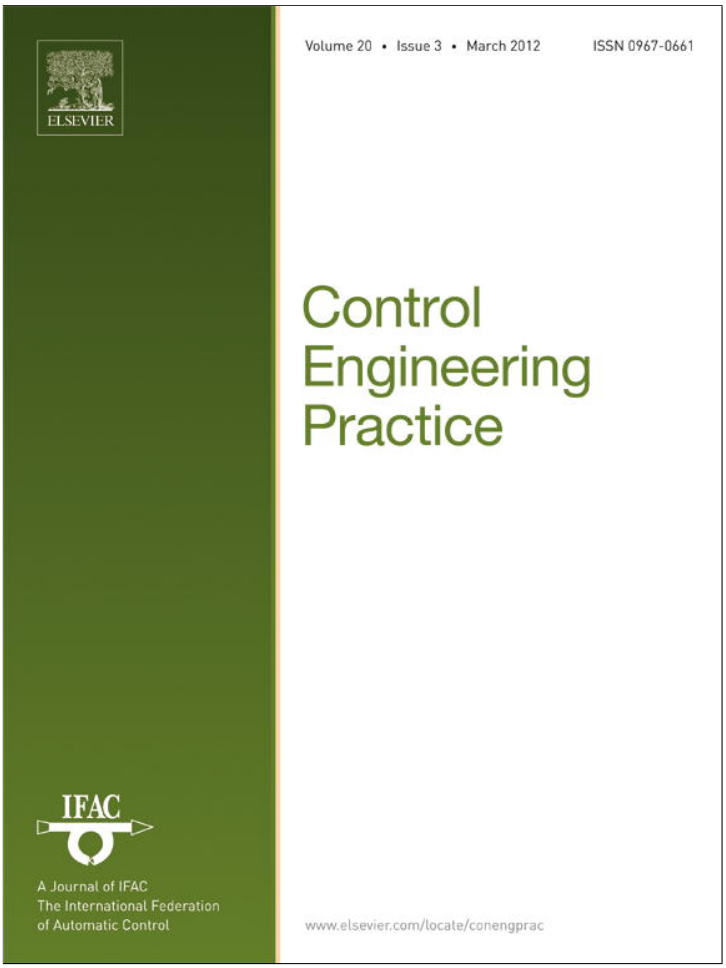

Control Engineering Practice 20 (2012) 315–325

Contents lists available at SciVerse ScienceDirect

Control Engineering Practice

journal homepage: www.elsevier.com/locate/conengprac

Switching algorithm for robust configuration control of a wheeled vehicle

Augie Widyotriatmo [a,1], Keum-Shik Hong [b,*]

[a] Instrumentation and Control Research Group, Bandung Institute of Technology, Ganesha 10, Bandung 40132, Indonesia
[b] Department of Cogno-Mechatronics Engineering and School of Mechanical Engineering, Pusan National University, 30 Jangjeon-dong, Geumjeong-gu, Busan 609-735, Korea

ARTICLE INFO

Article history:
Received 7 May 2010
Accepted 30 November 2011
Available online 26 December 2011

Keywords:
Configuration control
Forklift
Lyapunov method
Mobile robot
Robustness

ABSTRACT

In this paper, a robust configuration (i.e., position and orientation) control of an industrial forklift is investigated. The equations of motion of a typical forklift are derived. Configuration control utilizing three navigation variables (i.e., the distance to the goal point and two split angles of the orientation error) is designed. Considering that an industrial forklift should move forward and backward effectively depending on the location of a goal point, control laws with regard to forward and backward movements are separately derived. For a nominal model that does not include any uncertainty, the developed control law assures the uniform asymptotic stability. However, in the presence of uncertainties, the control law guarantees that the solutions of three navigation variables are uniformly bounded. The effectiveness of the developed algorithm is demonstrated through simulations and experiments.

1. Introduction

The configuration (i.e., position and orientation) control problem of autonomous wheeled vehicles has been widely studied over several years. The examples include the pallet-picking of an autonomous forklift, the recharging of an autonomous mobile robot, the parking of an autonomous car, and others. In modeling an autonomous system, there always occur uncertainties: tire/surface slip, measurement noise, gear backlash, friction, neglected vehicle dynamics, and more. In this paper, a robust configuration control problem of an autonomous forklift considering the above uncertainties is focused, in which the uncertainties are put into three categories: measurement noises, modeling errors, and tracking errors.

A wheeled vehicle is a nonholonomic system (i.e., a system with nonholonomic constraints). Brockett (1983) proved that a state-feedback control in the Cartesian coordinate system cannot be used to drive a nonholonomic system to an arbitrary configuration in an asymptotic fashion. To cope with this problem, coordinate transformations have been used. Their examples include the chained form (Murray & Sastry, 1993), the polar coordinates (Aicardi, Casalino, Bicchi, & Balestrino, 1995), the sigma process (Astolfi, 1996), and the transverse form (Morin & Samson, 2009). Other notable control strategies include the time-varying controls (Samson, 1995; Tamba, Hong, & Hong, 2009), discontinuous controls (Astolfi, 1996; Marchand & Alamir, 2003), the switching method (Hespanha & Morse, 1999), the model predictive control (Yoon, Shin, Kim, Park, & Sastry, 2009), the iterative-state steering controls (Lucibello & Oriolo, 2001; Widyotriatmo, Hong, & Hong, 2009), and the linear-interpolation-based control (Scaglia, Rosales, Quintero, Mut, & Agarwal, 2010). The configuration control designed in the polar coordinate is known to provide fast and natural motions from an initial to a goal configurations (Aicardi et al., 1995; Hong, Tamba, & Song, 2008; Oriolo, De Luca, & Vendittelli, 2002; Park, Yoo, Park, & Choi, 2009; Shim & Sung, 2004; Siegwart & Nourbakhsh, 2004; Widyotriatmo & Hong, 2011). It is also noted that most early works assumed the no slipping of wheels, no tracking errors, and no measurement noises.

As reported in Jiang (2000) and Widyotriatmo, Hong, and Prayudhi (2010), a supposedly ideal feedback law that regulates a mobile robot to a fixed configuration can diverge if even small uncertainties occur. Among the many studies that investigated the robustness of configuration control against uncertainties, some dealt with the identification of parametric uncertainties and modeling errors (Ge, Wang, & Lee, 2003; Lin & Yang, 2008), the switching schemes (Bui & Hong, 2010; Prieur & Astolfi, 2003; Xi, Feng, Jiang, & Cheng, 2003), the sliding mode controls (Corradini & Orlando, 2002; Floquet, Barbot, & Peruquetti, 2003), and the velocity scheduling control (Buccieri, Perritaz, Mullhaupt, Jiang, & Bonvin, 2009). Tang, Miller, Krovi, Ryu, and Agrawal (2008) and Ryu and Agrawal (2010) investigated the polynomial trajectory planning and control based on the differential flatness properties of a wheeled mobile robot. In path/trajectory tracking, the linear algebraic method (Ailon, Berman, & Arogeti, 2005), fuzzy controls (Moustris & Tzafestas, 2011; Treesatayapun, 2011), and adaptive controls (Martins, Celeste,

* Corresponding author. Tel.: +82 51 510 2454; fax: +82 51 514 0685.
E-mail addresses: augie@pusan.ac.kr (A. Widyotriatmo), kshong@pusan.ac.kr (K.-S. Hong).
[1] Tel.: +62 22 250 4424; fax: +62 22 250 6281.

0967-0661/$ - see front matter © 2011 Elsevier Ltd. All rights reserved.
doi:10.1016/j.conengprac.2011.11.007

Carelli, Sarcinelli-Filho, & Bastos-Filho, 2008; Rossomando, Soria, & Carelli, 2011) were utilized.

In the present paper, the use of two loops is proposed: the outer loop is to compute two desired control commands (linear velocity and steering angle of the driving wheel), and the inner loop is to track the two desired commands by applying the conventional proportional-derivative (PD) control to the two AC motors (one for driving and the other for steering). The outer loop incorporates all the noises, modeling errors, and tracking errors. In designing the control commands, three navigation variables (i.e., the distance error and two split angles of the orientation error, one in association with the direction to the goal point, and the other in association with the desired direction at the goal point) are utilized. Since the forklift can move freely in both directions (forward and backward), the workspace is split into two regions depending on the location of the goal point (whether it is located in front of the vehicle or not). For a nominal model (i.e., no noise and no uncertainty), a control law that assures the uniform asymptotic stability of the origin in the configuration error space is first proposed. And then a robust control law that guarantees the uniform boundedness of the solutions of three navigation variables in the presence of uncertainties (measurement noises, modeling errors, and tracking errors) is derived.

The contributions of this paper are the following. A control model of a typical forklift and its configuration control in the presence of input disturbances, measurement noises, and modeling errors are first discussed. If one goal configuration is assigned to individual vehicles, there exists only one equilibrium point to each vehicle.

Fig. 1. The forklift used in experiment.

Second, control laws that assure the uniform asymptotic stability, when there is no uncertainty, and the uniform boundedness, in the presence of uncertainties, of the equilibrium point are proposed. Third, a discrete-time analysis for the proposed algorithm and the range of control gains in terms of sampling time are clarified. Fourth, experimental results using an autonomous forklift are provided.

The paper has the following structure. Section 2 describes the overall control structure, derives the equations of motion, analyzes the AC motor control, and formulates the configuration control problem for forward and backward movements. Section 3 discusses the proposed control laws for the ideal case and in the presence of uncertainties. Section 4 presents the stability analysis of the proposed control laws in the discrete-time domain. Section 5 provides simulation and experimental results confirming the effectiveness of the proposed method for driving the forklift from an arbitrary initial configuration to a desired goal configuration. Section 6 draws conclusions.

2. Autonomous forklift model

2.1. Control structure

Fig. 1 depicts the developed autonomous forklift having two caster wheels in the front and one drivable-and-steerable wheel in the rear. It is equipped with a laser-based localization sensor SICK NAV200, an embedded PC, and a programmable logic controller (PLC). The NAV200 is used to measure the position (x, y) and orientation (θ) of the forklift in the global coordinate frame based upon the known locations of reflectors. Fig. 2 shows a control block diagram of the forklift having two loops: outer loop and inner loop. The outer loop, programmed in C++ on an industrial PC, generates two desired commands: the linear velocity (v_d) and the steering angle (δ_d) of the driving wheel. These commands are updated upon the errors between the goal configuration (x_g, y_g, θ_g) and the present configuration $(x(t), y(t), \theta(t))$ measured by NAV200 at a sampling frequency of 10 Hz. The inner loop, implemented in the PLC, generates two control signals (voltages u_v and u_δ) to control the two AC motors (driving and steering) in the fashion that the driving wheel follows the desired commands. The two voltages are calculated using the desired commands and the encoders' feedback at the frequency of 100 Hz. The PLC and the industrial PC communicates via RS232.

2.2. Equations of motion

Fig. 3 shows a schematic of the forklift. O-$\hat{i}\hat{j}$ represents the global reference coordinate frame in the workspace; O_b-$\hat{i}_b\hat{j}_b$ denotes the body coordinate frame attached to the vehicle body where O_b (the

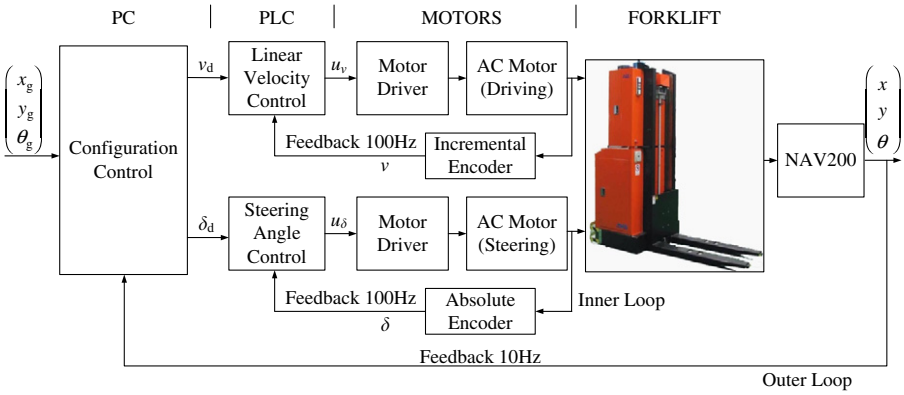

Fig. 2. Control block diagram.

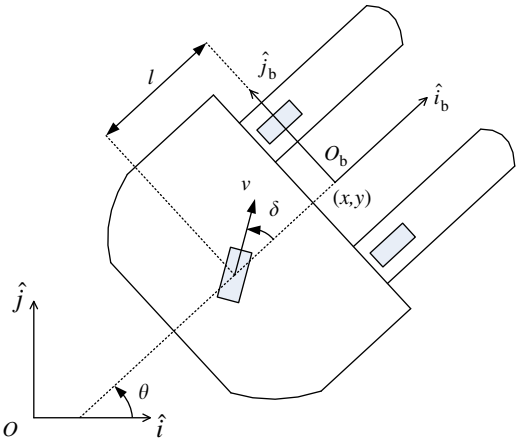

Fig. 3. Forklift schematic.

mid-point of two front wheels) is the origin of the frame to which all the motions of the vehicle are generated; and l denotes the distance between the center of the rear wheel and O_b. The vehicle's configuration is specified by its position (x, y) and orientation θ, which is the angle of the $\hat{i}_b$-axis from the $\hat{i}$-axis (in the counterclockwise direction). The velocity v and angle δ in $(-\pi,\pi)$ are the linear velocity and the steering angle of the rear wheel from the $\hat{i}_b$-axis, respectively.

Let φ_f and φ_r be the angular displacements of the front and rear wheels, respectively. Let $\mathbf{p}=[x,y,\theta,\delta,\varphi_f,\varphi_r]^T \in R^6$ be the state vector. Then, the equations of motion and nonholonomic constraints of the vehicle are given as follows (Fierro & Lewis, 1998):

$$\mathbf{M}(\mathbf{p})\ddot{\mathbf{p}}+\mathbf{C}(\mathbf{p},\ \dot{\mathbf{p}})\dot{\mathbf{p}}+\mathbf{f}+\mathbf{g}(\mathbf{p})=\mathbf{B}(\mathbf{p})\boldsymbol{\tau}+\mathbf{J}(\mathbf{p})\mathbf{f}_C, \tag{1}$$

$$\mathbf{J}^T(\mathbf{p})\dot{\mathbf{p}}=\mathbf{0}, \tag{2}$$

where $\mathbf{M}(\mathbf{p})\in R^{6\times 6}$ is the symmetric and positive definite inertia matrix, $\mathbf{C}(\mathbf{p},\ \dot{\mathbf{p}})\in R^{6\times 6}$ is the centripetal and Coriolis matrix, $\mathbf{f}\in R^6$ is the surface friction vector, $\mathbf{g}(\mathbf{p})\in R^6$ is the gravitational vector, $\mathbf{B}(\mathbf{p})\in R^{6\times 2}$ is the input matrix, $\boldsymbol{\tau}=[\tau_v,\ \tau_\delta]^T\in R^2$ is the torque inputs to the driving and steering motors, respectively, $\mathbf{f}_C\in R^4$ is the constraint force vector, and $\mathbf{J}(\mathbf{p})\in R^{6\times 4}$ is the constraint matrix. In this paper, it is assumed that the vehicle operates on a flat surface, so that $\mathbf{g}(\mathbf{p})=\mathbf{0}$. In driving the ideal model, it is also assumed that the vehicle satisfies the conditions of nonslipping (or pure) rolling. Then, the constraint matrix $\mathbf{J}(\mathbf{p})$ is given by

$$\mathbf{J}(\mathbf{p})=\begin{bmatrix} -\sin\theta & -(\cos\theta\sin\delta+\sin\theta\cos\delta) & \cos\theta & \cos\theta\cos\delta-\sin\theta\sin\delta \\ \cos\theta & \cos\theta\cos\delta-\sin\theta\sin\delta & \sin\theta & \cos\theta\sin\delta+\sin\theta\cos\delta \\ 0 & -l\cos\delta & 0 & -l\sin\delta \\ 0 & 0 & 0 & 0 \\ 0 & 0 & -r_f & 0 \\ 0 & 0 & 0 & -r_r \end{bmatrix}, \tag{3}$$

where r_f and r_r are the radii of the front and rear wheels, respectively. A matrix $\mathbf{S}(\mathbf{p})\in R^{6\times 2}$, to obtain $\mathbf{S}^T(\mathbf{p})\mathbf{J}(\mathbf{p})=0$, is chosen as

$$\mathbf{S}(\mathbf{p})=\begin{bmatrix} \cos\theta\cos\delta & \sin\theta\cos\delta & -(1/l)\sin\delta & 0 & (1/r_f)\cos\delta & 1/r_r \\ 0 & 0 & 0 & 1 & 0 & 0 \end{bmatrix}^T. \tag{4}$$

Let $\dot{\delta}$ be the angular velocity of the steering angle. Let $\mathbf{v}=[v,\ \dot{\delta}]^T$. Then, the first derivative of vector $\mathbf{p}$ is obtained as

$$\dot{\mathbf{p}}=\mathbf{S}(\mathbf{p})\mathbf{v} =\begin{bmatrix} \cos\theta\cos\delta & \sin\theta\cos\delta & -(1/l)\sin\delta & 0 & (1/r_f)\cos\delta & 1/r_r \\ 0 & 0 & 0 & 1 & 0 & 0 \end{bmatrix}^T \begin{bmatrix} v \\ \dot{\delta} \end{bmatrix}. \tag{5}$$

Now, using the Lagrange method, the specific forms of (1) are derived. The kinetic energy K is given by

$$K=\frac{1}{2}\dot{\mathbf{p}}^T\mathbf{M}\dot{\mathbf{p}}, \tag{6}$$

$$\mathbf{M}=\begin{bmatrix} m & 0 & 0 & 0 & 0 & 0 \\ 0 & m & 0 & 0 & 0 & 0 \\ 0 & 0 & I_b & 0 & 0 & 0 \\ 0 & 0 & 0 & I_\delta & 0 & 0 \\ 0 & 0 & 0 & 0 & I_f & 0 \\ 0 & 0 & 0 & 0 & 0 & I_r \end{bmatrix}, \tag{7}$$

where m is the vehicle mass, I_b is the mass moment of inertia of the vehicle with respect to O_b, I_δ is that of the rear wheel with respect to the normal axis to the flat surface, and I_f and I_r are the mass moments of inertia of the front and rear wheels around their individual rolling axes. The centripetal and Coriolis matrix $\mathbf{C}(\mathbf{p},\ \dot{\mathbf{p}})$ is given by

$$\mathbf{C}(\mathbf{p},\dot{\mathbf{p}})=\dot{\mathbf{M}}(\mathbf{p})\dot{\mathbf{p}}-\frac{\partial K}{\partial \mathbf{p}}=0. \tag{8}$$

The input matrix $\mathbf{B}(\mathbf{p})$ is

$$\mathbf{B}(\mathbf{p})=\begin{bmatrix} 0 & 0 & 0 & 0 & 0 & 1 \\ 0 & 0 & 0 & 1 & 0 & 0 \end{bmatrix}^T. \tag{9}$$

From (5), the second derivative of vector $\mathbf{p}$ is obtained as

$$\ddot{\mathbf{p}}=\mathbf{S}(\mathbf{p})\dot{\mathbf{v}}+\dot{\mathbf{S}}(\mathbf{p},\dot{\mathbf{p}})\mathbf{v}. \tag{10}$$

The substitution of (10) into (1) and multiplication of $\mathbf{S}^T(\mathbf{p})$ at both sides yields

$$\mathbf{M}_1(\mathbf{p})\dot{\mathbf{v}}+\mathbf{C}_1(\mathbf{p},\dot{\mathbf{p}})\mathbf{v}+\mathbf{f}_1=\mathbf{B}_1(\mathbf{p})\boldsymbol{\tau}, \tag{11}$$

where

$$\mathbf{M}_1(\mathbf{p})=\mathbf{S}^T(\mathbf{p})\mathbf{M}(\mathbf{p})\mathbf{S}(\mathbf{p}) =\begin{bmatrix} (m+(I_f/r_f^2))\cos^2\delta+(I_b/l^2)\sin^2\delta+I_r & 0 \\ 0 & I_\delta \end{bmatrix}, \tag{12}$$

$$\mathbf{C}_1(\mathbf{p},\dot{\mathbf{p}})=\mathbf{S}^T(\mathbf{p})\mathbf{M}(\mathbf{p})\dot{\mathbf{S}}(\mathbf{p},\dot{\mathbf{p}}) =\begin{bmatrix} ((I_b/l^2)-(m+(I_f/r_f^2)))\cos\delta\sin\delta\dot{\delta} & 0 \\ 0 & 0 \end{bmatrix}, \tag{13}$$

$$\mathbf{f}_1=\mathbf{S}^T(\mathbf{p})\mathbf{f}=\begin{bmatrix} f_v & f_\delta \end{bmatrix}^T, \tag{14}$$

$$\mathbf{B}_1(\mathbf{p})=\begin{bmatrix} 1/r_r & 0 \\ 0 & 1 \end{bmatrix}. \tag{15}$$

Note that f_v and f_δ are the surface frictions against the linear and rotational motions of the rear wheel, respectively. Finally, the equations of motion for the forklift in Fig. 3 are

$$\dot{x}=v\cos\theta\cos\delta, \tag{16}$$

$$\dot{y}=v\sin\theta\cos\delta, \tag{17}$$

$$\dot{\theta}=-(v/l)\sin\delta, \tag{18}$$

$$m_1\dot{v}+c_1v+r_rf_v=\tau_v, \tag{19}$$

$$I_\delta\ddot{\delta}+f_\delta=\tau_\delta, \tag{20}$$

where

$$m_1=r_r((m+(I_f/r_f^2))\cos^2\delta+(I_b/l^2)\sin^2\delta+I_r), \tag{21}$$

$$c_1=r_r((I_b/l^2)-(I_f/r_f^2)-m)\cos\delta\sin\delta\dot{\delta}, \tag{22}$$

and I_δ is mass moment of the rear wheel and τ_v, τ_δ are the torque inputs to the driving and steering motors.

2.3. AC motor control

In this subsection, the dynamics of the vehicle in (19) and (20) are focused. Assuming that the inductance voltages of the motors are negligible, the torques of the driving motor τ_v and the steering motor τ_δ are obtained as (De La Cruz, Bastos, & Carelli, 2011)

$$\tau_v = (k_{m,v}/R_{m,v})((u_v - (k_{\mathrm{emf},v}/r_\mathrm{r})v), \tag{23}$$

$$\tau_\delta = (k_{m,\delta}/R_{m,\delta})(u_\delta - k_{\mathrm{emf},\delta}\dot{\delta}), \tag{24}$$

where u_v and u_δ are the input voltages applied to the driving and steering motors, respectively, and $k_{m,v}$, $k_{\mathrm{emf},v}$, and $R_{m,v}$ are the motor torque constant, the back electromotive constant multiplied by a gear ratio, and the resistance of the driving motor, respectively, and $k_{m,\delta}$, $R_{m,\delta}$, and $k_{\mathrm{emf},\delta}$ are those of the steering motor, respectively.

To track the desired linear velocity v_d and steering angle δ_d, a PD control is adopted. The control signals u_v and u_δ are designed as

$$u_v = k_{P,v}(v_\mathrm{d} - v) - k_{D,v}\dot{v}, \tag{25}$$

$$u_\delta = k_{P,\delta}(\delta_\mathrm{d} - \delta) - k_{D,\delta}\dot{\delta}, \tag{26}$$

where $k_{P,v}$ and $k_{D,v}$ are the proportional and the derivative gains of the driving motor, and $k_{P,\delta}$ and $k_{D,\delta}$ are those of the steering motor, respectively. Using (23) and (25), (19) becomes

$$\begin{aligned}&((R_{m,v}/k_{m,v})m_1 + k_{D,v})\dot{v} + ((R_{m,v}/k_{m,v})c_1 + k_{\mathrm{emf},v}/r_\mathrm{r} + k_{P,v})v\\ &\quad = k_{P,v}v_\mathrm{d} - (R_{m,v}r_\mathrm{r}/k_{m,v})f_v.\end{aligned} \tag{27}$$

Choosing $k_{P,v} > \max((R_{m,v}/k_{m,v})c_1 - k_{\mathrm{emf},v}/r_\mathrm{r})$ and assuming that f_v is constant, the solution of (27) is obtained as

$$\begin{aligned}v(t) = {}&(k_{P,v}/((R_{m,v}/k_{m,v})c_1 + k_{\mathrm{emf},v}/r_\mathrm{r} + k_{P,v}))\\ &\times(v_\mathrm{d} - ((R_{m,v}r_\mathrm{r})/(k_{m,v}k_{P,v}))f_v\\ &-(v_\mathrm{d} - v(t_0) - ((R_{m,v}r_\mathrm{r})/(k_{m,v}k_{P,v}))f_v))\exp(-\lambda_v t),\end{aligned} \tag{28}$$

where

$$\lambda_v = ((R_{m,v}/k_{m,v})c_1 + k_{\mathrm{emf},v}/r_\mathrm{r} + k_{P,v})/((R_{m,v}/k_{m,v})m_1 + k_{D,v}) > 0. \tag{29}$$

Now, the substitution of (24) and (26) into (20) yields

$$\begin{aligned}&(R_{m,\delta}/(k_{m,\delta}k_{P,\delta}))I_\delta\ddot{\delta} + ((k_{D,\delta} + k_{\mathrm{emf},\delta})/k_{P,\delta})\dot{\delta} + \delta\\ &\quad = \delta_\mathrm{d} - (R_{m,\delta}/(k_{m,\delta}k_{P,\delta}))f_\delta.\end{aligned} \tag{30}$$

An overdamped response of the steering angle δ is designed by setting $k_{P,\delta}$ and $k_{D,\delta}$ such that

$$((k_{D,\delta} + k_{\mathrm{emf},\delta})/k_{P,\delta})^2 - 4(R_{m,\delta}I_\delta)/(k_{m,\delta}k_{P,\delta}) > 0. \tag{31}$$

Assuming that f_δ is constant, the solution of (30) becomes

$$\begin{aligned}\delta(t) = {}&\delta_\mathrm{d} - (R_{m,\delta}/(k_{m,\delta}k_{P,\delta}))f_\delta\\ &-(\delta_\mathrm{d} - \delta(t_0) - (R_{m,\delta}/(k_{m,\delta}k_{P,\delta}))f_\delta)\frac{\lambda_{\delta,2}\exp(-\lambda_{\delta,1}t) - \lambda_{\delta,1}\exp(-\lambda_{\delta,2}t)}{\lambda_{\delta,2} - \lambda_{\delta,1}},\end{aligned} \tag{32}$$

where

$$\begin{aligned}\lambda_{\delta,1} &= \frac{((k_{D,\delta} + k_{\mathrm{emf},\delta})/k_{P,\delta}) + \sqrt{((k_{D,\delta} + k_{\mathrm{emf},\delta})/k_{P,\delta})^2 - 4(R_{m,\delta}I_\delta)/(k_{m,\delta}k_{P,\delta})}}{2(R_{m,\delta}I_\delta)/(k_{m,\delta}k_{P,\delta})} > 0,\\ \lambda_{\delta,2} &= \frac{((k_{D,\delta} + k_{\mathrm{emf},\delta})/k_{P,\delta}) - \sqrt{((k_{D,\delta} + k_{\mathrm{emf},\delta})/k_{P,\delta})^2 - 4(R_{m,\delta}I_\delta)/(k_{m,\delta}k_{P,\delta})}}{2(R_{m,\delta}I_\delta)/(k_{m,\delta}k_{P,\delta})} > 0.\end{aligned} \tag{33}$$

From (28) and (32), the linear velocity v and the steering angle δ track the desired commands v_d and δ_d with tracking errors $\tilde{v} = v - v_\mathrm{d}$ and $\tilde{\delta} = \delta - \delta_\mathrm{d}$ caused by the frictions and the exponential terms in (28) and (32). The time constants of the exponential term of the linear velocity and of the steering angle are $1/\lambda_v$ and $1/\lambda_{\delta,2}$, respectively. As the load of the forklift m increases, the exponential terms decay slowly, and therefore the two tracking errors ($\tilde{v}$ and $\tilde{\delta}$) also increase. In this paper, it is assumed that the load variation during motions is very small and using the fixed gains of PD control, the linear velocity v and steering angle δ can track their desired values v_d and δ_d with small bounded tracking errors $|\tilde{v}| \le \bar{\tilde{v}}$ and $|\tilde{\delta}| \le \bar{\tilde{\delta}}$, where $\bar{\tilde{v}}$ and $\bar{\tilde{\delta}}$ are their bounds.

2.4. Kinematic equations in navigation variables

Fig. 4(a) and (b) illustrates two situations: (a) the case that a forward movement of the forklift is quicker to reach the goal position and (b) the case that a backward movement is quicker, which is the case that the goal position is located behind the vehicle. The goal coordinate frame O_g–$\hat{i}_\mathrm{g}\hat{j}_\mathrm{g}$ is set to the desired goal configuration of

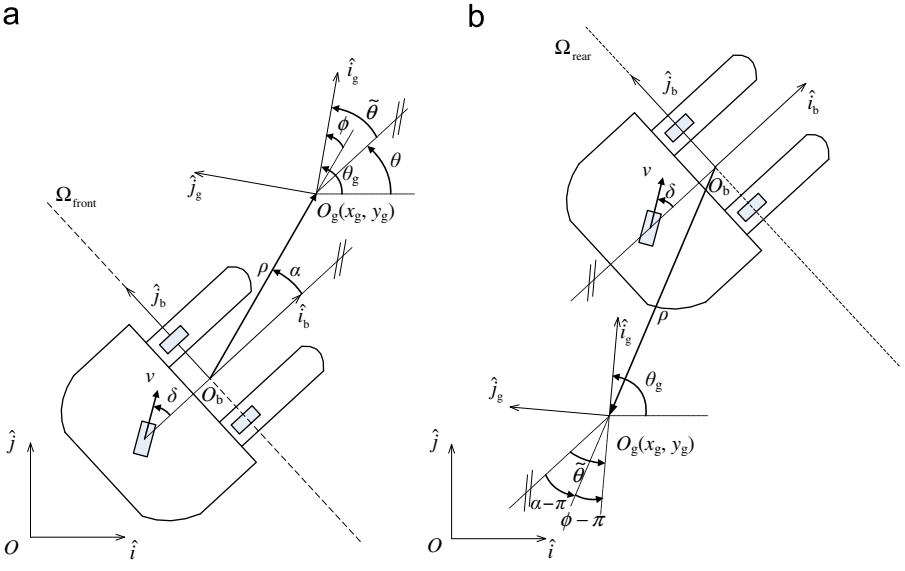

Fig. 4. The introduced navigation variables $\{\rho, \alpha, \phi\}$ and two regions for determining the initial moving direction of the vehicle: (a) Ω_{front} for forward movement and (b) Ω_{rear} for backward movement.

the vehicle at the goal point, where (x_g,y_g) is the coordinates of the goal point O_g, and θ_g is the rotational angle of the $\hat{i}_g$-axis from the global $\hat{i}$-axis. Let $\tilde{x}=x_g-x$, $\tilde{y}=y_g-y$, and $\tilde{\theta}=\theta_g-\theta$ be the configuration errors between the current and goal configurations. Now, three new navigation variables $\{\rho, \alpha, \phi\}$ are defined as follows:

$$\rho=\sqrt{\tilde{x}^2+\tilde{y}^2}, \tag{34}$$

$$\alpha=\arctan 2(\tilde{y},\tilde{x})-\theta, \tag{35}$$

$$\phi=\theta_g-\arctan 2(\tilde{y},\tilde{x}), \tag{36}$$

where ρ is the distance error, and α and ϕ are the split portions of the orientation error (i.e., $\tilde{\theta}=\alpha+\phi$), in which α is the portion from the vehicle's moving direction to the goal point direction and ϕ is the remaining error at the goal frame. It is noted that α and ϕ are not defined if $\tilde{x}=\tilde{y}=0$ (i.e., $\rho=0$). In determining the initial moving direction (forward or backward) of the vehicle upon receiving a command, two regions (Ω_{front} and Ω_{rear}) are defined as

$$\Omega_{\text{front}}=\{(x_g, y_g): \quad |\arctan 2(y_g-y,x_g-x)-\theta|<\pi/2\}, \tag{37}$$

$$\Omega_{\text{rear}}=\{(x_g, y_g): \quad |\arctan 2(y_g-y,x_g-x)-\theta|>\pi/2\}. \tag{38}$$

Then, the kinematic Eqs. (16)–(18) using the introduced navigation variables become

$$\dot{\rho}=-v\cos\alpha\cos\delta, \tag{39}$$

$$\dot{\alpha}=(v/\rho)\sin\alpha\cos\delta+(v/l)\sin\delta, \tag{40}$$

$$\dot{\phi}=-(v/\rho)\sin\alpha\cos\delta. \tag{41}$$

If the vehicle achieves its goal configuration, both ρ and $\tilde{\theta}$ $(\alpha+\phi)$ become zero. Let the polar coordinate system comprising ρ and $\tilde{\theta}$ be the error space. The control problem of moving a vehicle from an initial configuration to a goal configuration becomes the asymptotic stabilization problem from an arbitrary point in the error space to its origin. It is noted that $\tilde{\theta}=0$ is achieved by making $\alpha=\phi=0$ in Ω_{front}, but that is achieved by making $\alpha=\phi=\pi$ in Ω_{rear}. Therefore, the target points become $(\rho,\alpha,\phi)=(0,0,0)$ in Ω_{front} and $(\rho,\alpha,\phi)=(0,\pi,\pi)$ in Ω_{rear}.

3. Control laws design

3.1. Control law for the ideal case

In this subsection, the control laws that achieve the asymptotic stability of the equilibrium points (i.e., (0, 0, 0) if $(x_g,y_g)\in\Omega_{\text{front}}$ and $(0, \pi, \pi)$ if $(x_g, y_g)\in\Omega_{\text{rear}}$) for the nominal model (39)–(41) are derived. The tracking errors ($\tilde{v}$ and $\tilde{\delta}$) are assumed to be negligible, so that $v=v_d$ and $\delta=\delta_d$ (the control laws under uncertainties will be discussed in Section 3.2). The control law in Ω_{front} is first derived. Let $v_1=v\cos\delta$ and $v_2=v\sin\delta$. Then, v and δ in terms of v_1 and v_2, respectively, become

$$v=\text{sgn}(v_1)\sqrt{v_1^2+v_2^2}, \tag{42}$$

$$\delta=\arctan(v_2/v_1). \tag{43}$$

Let $\alpha'=\sin\alpha-\phi$. Let v_1 and v_2 be designed as

$$v_1=k_{v,1}\rho\sqrt{1-(\alpha'+\phi)^2}, \tag{44}$$

$$v_2=-l(k_{v,2}\alpha'+k_{v,1}\phi\sqrt{1-(\alpha'+\phi)^2}), \tag{45}$$

where $k_{v,1}$ and $k_{v,2}$ are positive constant gains. From (39)–(41) and (42)–(45), the following are obtained:

$$\dot{\rho}=-k_{v,1}\rho(1-(\alpha'+\phi)^2), \tag{46}$$

$$\dot{\alpha}'=-\left(\left(k_{v,2}-k_{v,1}\left(1+\sqrt{1-(\alpha'+\phi)^2}\right)\right)\sqrt{1-(\alpha'+\phi)^2}\right)\alpha' + \left(k_{v,1}\sqrt{1-(\alpha'+\phi)^2}\right)\phi, \tag{47}$$

$$\dot{\phi}=-\left(k_{v,1}\sqrt{1-(\alpha'+\phi)^2}\right)\alpha'-\left(k_{v,1}\sqrt{1-(\alpha'+\phi)^2}\right)\phi. \tag{48}$$

Let $\varsigma_\alpha=\left(k_{v,2}-k_{v,1}\left(1+\sqrt{1-(\alpha'+\phi)^2}\right)\right)\sqrt{1-(\alpha'+\phi)^2}$ and $\varsigma_\phi=k_{v,1}\sqrt{1-(\alpha'+\phi)^2}>0$. Note that $\varsigma_\alpha>0$ is achieved if $k_{v,2}>2k_{v,1}$.

Let a Lyapunov function candidate be

$$V=(1/2)(\rho^2+\alpha'^2+\phi^2). \tag{49}$$

Using (46)–(48), the time derivative of V becomes

$$\dot{V}=-(\varsigma_\phi^2/k_{v,1})\rho^2-\varsigma_\alpha\alpha'^2-\varsigma_\phi\phi^2. \tag{50}$$

Theorem 1. *Consider the system* (39)–(41) *with goal points in* Ω_{front}. *Let the control law be given by*

$$v=\sqrt{(k_{v,1}\rho\cos\alpha)^2+l^2(k_{v,2}\sin\alpha-(k_{v,2}-k_{v,1}\cos\alpha)\phi)^2}, \tag{51}$$

$$\delta=-\arctan\left(l\left(\frac{k_{v,2}\sin\alpha-(k_{v,2}-k_{v,1}\cos\alpha)\phi}{k_{v,1}\rho\cos\alpha}\right)\right), \tag{52}$$

where $k_{v,2}>2k_{v,1}>0$. *Then, the origin* $(\rho, \alpha, \phi)=(0, 0, 0)$ *is uniformly asymptotically stable.*

Proof. Let $(x_g,y_g)\in\Omega_{\text{front}}$, (50) is rewritten as

$$\dot{V}=-(\varsigma_\phi^2/k_{v,1})\rho^2-\varsigma_\alpha(\sin\alpha-\phi)^2-\varsigma_\phi\phi^2 \quad \le 0, \tag{53}$$

where ς_ϕ, $\varsigma_\alpha>0$ if $k_{v,2}>2k_{v,1}>0$. Based on Barbalat's lemma (Khalil, 2002; p. 323), (53) concludes that $\rho,\alpha,\phi\to 0$ as $t\to\infty$. □

Corollary 1. *Consider the system* (39)–(41) *with goal points in* Ω_{rear}. *Let the control law be*

$$v=-\sqrt{(k_{v,1}\rho\cos\alpha)^2+l^2(k_{v,2}\sin\alpha+(k_{v,2}+k_{v,1}\cos\alpha)(\phi-\pi))^2}, \tag{54}$$

$$\delta=-\arctan\left(l\left(\frac{k_{v,2}\sin\alpha+(k_{v,2}+k_{v,1}\cos\alpha)(\phi-\pi)}{k_{v,1}\rho\cos\alpha}\right)\right). \tag{55}$$

Then, $(\rho, \alpha, \phi)=(0, \pi, \pi)$ *is uniformly asymptotically stable.*

Proof. Using the same procedure as in (44)–(48), the time-derivative of the Lyapunov function candidate $V=(1/2)(\rho^2+(\sin(\alpha-\pi)-(\phi-\pi))^2+(\phi-\pi)^2)$ for $(x_g,y_g)\in\Omega_{\text{rear}}$ is obtained as

$$\dot{V}=-(\varsigma_{\phi-\pi}^2/k_{v,1})\rho^2-\varsigma_{\alpha-\pi}(\sin(\alpha-\pi)-(\phi-\pi))^2-\varsigma_{\phi-\pi}(\phi-\pi)^2\le 0, \tag{56}$$

where $\varsigma_{\alpha-\pi}=(k_{v,2}-k_{v,1}(1+\cos(\alpha-\pi)))\cos(\alpha-\pi)>0$ and $\varsigma_{\phi-\pi}=k_{v,1}\cos(\alpha-\pi)>0$ in Ω_{rear}. Therefore, $\rho\to 0$ and $\alpha,\phi\to\pi$ as $t\to\infty$. □

Remark 1. As noted in Section 2.4, if $\rho=0$, α and ϕ are not defined. In this special case, let v and δ be determined as

$$v=k_{v,1}|\tilde{\theta}|, \tag{57}$$

$$\delta=-(\pi/2)\text{sgn}\tilde{\theta}. \tag{58}$$

The substitution of (57) and (58) into (16)–(18) yields

$$\dot{\tilde{x}}=0, \tag{59}$$

$$\dot{\tilde{y}}=0, \tag{60}$$

$$\dot{\tilde{\theta}} = -k_{v,1}\tilde{\theta}. \tag{61}$$

Then, the orientation error $\tilde{\theta}$ converges exponentially to zero while the position error $(\tilde{x}, \tilde{y})$ remains at zero.

Remark 2. $\alpha' + \phi = 1$ (or $\alpha = \pm\pi/2$) results in equilibrium points of (46)–(48). To get out from the equibrium point, the linear velocity v is chosen as a nonzero constant v_ε for a short time interval [0, t_ε). Once the state escapes from $\alpha(t_\varepsilon) = \pm\pi/2$, the linear velocity and steering angle are set to (51) and (52) if $(x_g, y_g) \in \Omega_{\text{front}}$ or to (54) and (55) if $(x_g, y_g) \in \Omega_{\text{rear}}$.

Remark 3. The gains $k_{v,1}$ and $k_{v,2}$ can be chosen via the linearization of (46)–(48) at the origin, in which the spectrum of the linearized system can be assigned by proper $k_{v,1}$ and $k_{v,2}$.

3.2. Control laws in the presence of uncertainties

The kinematic Eqs. (39)–(41) were obtained under the very ideal conditions (no slipping, accurate measurement, precise tracking, and others). In real environments, there always exist uncertainties: measurement noises, modeling errors, and tracking errors. Let (n_x, n_y) and n_θ be the measurement noises in (x, y) and θ, respectively, such that $|n_x| \le \overline{n}_x$, $|n_y| \le \overline{n}_y$, and $|n_\theta| \le \overline{n}_\theta$, where $\overline{n}_x$, $\overline{n}_y$, and $\overline{n}_\theta$ are their bounds. Then, the noises in the navigation variables are bounded by

$$|n_\rho| \le |\sqrt{(\tilde{x}+\overline{n}_x)^2 + (\tilde{y}+\overline{n}_y)^2} - \sqrt{\tilde{x}^2+\tilde{y}^2}|, \tag{62}$$

$$|n_\alpha| \le |\text{atan2}(\tilde{y}+\overline{n}_y, \tilde{x}+\overline{n}_x) - \text{atan2}(\tilde{y},\tilde{x})| + \overline{n}_\theta, \tag{63}$$

$$|n_\varphi| \le |\text{atan2}(\tilde{y}+\overline{n}_y, \tilde{x}+\overline{n}_x) - \text{atan2}(\tilde{y},\tilde{x})|. \tag{64}$$

Let Δ_i, $i \in \{\rho,\alpha,\phi\}$, be the possible modeling errors that satisfy $|\Delta_i| \le \overline{k}_i$ where $\overline{k}_i$ are positive constants. The kinematic Eqs. (39)–(41) including measurement noises, modeling errors, and tracking errors are written as

$$\dot{\rho} = -(v_d(\rho,\alpha,\phi;n_i)+\tilde{v})\cos\alpha\cos(\delta_d(\rho,\alpha,\phi;n_i)+\tilde{\delta}) + \Delta_\rho, \tag{65}$$

$$\dot{\alpha} = ((v_d(\rho,\alpha,\phi;n_i)+\tilde{v})/\rho)\sin\alpha\cos(\delta_d(\rho,\alpha,\phi;n_i)+\tilde{\delta}) + ((v_d(\rho,\alpha,\phi;n_i)+\tilde{v})/l)\sin(\delta_d(\rho,\alpha,\phi;n_i)+\tilde{\delta}) + \Delta_\alpha, \tag{66}$$

$$\dot{\varphi} = -((v_d(\rho,\alpha,\phi;n_i)+\tilde{v})/\rho)\sin\alpha\cos(\delta_d(\rho,\alpha,\phi;n_i)+\tilde{\delta}) + \Delta_\varphi, \tag{67}$$

where n_i, $i \in \{\rho,\alpha,\phi\}$, are the noises in the navigation variables.

Let $v_d = \text{sgn}(v_1)\sqrt{v_1^2+v_2^2}$ and $\delta_d = \arctan(v_2/v_1)$, and v_1 and v_2 be chosen as

$$v_1 = k_{v,1}\rho\sqrt{1-(\alpha'+\phi)^2} + v_1', \tag{68}$$

$$v_2 = -l(k_{v,2}\alpha' + k_{v,1}\phi\sqrt{1-(\alpha'+\phi)^2} - v_2'), \tag{69}$$

where v_1' and v_2' are functions to be designed. Using (65)–(67) and (68) and (69), the following are obtained:

$$\dot{\rho} = -k_{v,1}\rho(1-(\alpha'+\phi)^2) - (v_1'+\mu_1)\sqrt{1-(\alpha'+\phi)^2} + \Delta_\rho, \tag{70}$$

$$\dot{\alpha}' = -\left(\left(k_{v,2} - k_{v,1}\left(1-\sqrt{1-(\alpha'+\phi)^2}\right)\right)\sqrt{1-(\alpha'+\phi)^2}\right)\alpha' + \left(k_{v,1}\sqrt{1-(\alpha'+\phi)^2}\right)\phi + ((v_1'+\mu_1)/\rho)(\alpha'+\phi)\left(1+\sqrt{1-(\alpha'+\phi)^2}\right) + (v_2'+\mu_2)\sqrt{1-(\alpha'+\phi)^2} + \sqrt{1-(\alpha'+\phi)^2}\Delta_\alpha + \Delta_\phi, \tag{71}$$

$$\dot{\phi} = -\left(k_{v,1}\sqrt{1-(\alpha'+\phi)^2}\right)\alpha' - \left(k_{v,1}\sqrt{1-(\alpha'+\phi)^2}\right)\phi - ((v_1'+\mu_1)/\rho)(\alpha'+\phi) + \Delta_\phi, \tag{72}$$

where μ_1 and μ_2 are the bounded perturbations from the measurement noises and tracking errors such that $|\mu_1| \le \overline{\mu}_1$ and $|\mu_2| \le \overline{\mu}_2$, and $\overline{\mu}_1$ and $\overline{\mu}_2$ are their bounds. Let $\mathbf{w}$ be defined as

$$\mathbf{w} = \begin{bmatrix} w_1 \\ w_2 \end{bmatrix} = \begin{bmatrix} (\varsigma_\phi/k_{v,1})(-\rho^2 + (\alpha'^2 - \phi^2)) + (\alpha'+\phi)\alpha' \\ (\varsigma_\phi/k_{v,1})\alpha' \end{bmatrix}, \tag{73}$$

and v_1' and v_2' be designed as follows:

$$v_1' = \begin{cases} -k_{v,3}w_1/\|\mathbf{w}\|_2, & \text{if } k_{v,3}\|\mathbf{w}\|_2 \ge \varepsilon, \\ -k_{v,3}^2 w_1/\varepsilon, & \text{if } k_{v,3}\|\mathbf{w}\|_2 < \varepsilon, \end{cases} \tag{74}$$

$$v_2' = \begin{cases} -k_{v,3}w_2/\|\mathbf{w}\|_2, & \text{if } k_{v,3}\|\mathbf{w}\|_2 \ge \varepsilon, \\ -k_{v,3}^2 w_2/\varepsilon, & \text{if } k_{v,3}\|\mathbf{w}\|_2 < \varepsilon, \end{cases} \tag{75}$$

where $k_{v,3}$ is a positive constant gain such that $k_{v,3} \ge \sqrt{\overline{\mu}_1^2 + \overline{\mu}_2^2}$, and ε is a small positive constant. The second terms of v_1' in (74) and v_2' in (75) are chosen to avoid a possible division by zero. If $k_{v,3}\|\mathbf{w}\|_2 \ge \varepsilon$, the time-derivative of the Lyapunov function V in (49) becomes

$$\dot{V} \le -(\min(\varsigma_\phi^2/k_{v,1}, \varsigma_\alpha, \varsigma_\phi) - \max(\overline{k}_\rho, \overline{k}_\alpha + \overline{k}_\phi))(\rho^2 + \alpha_2'^2 + \phi^2) - |k_{v,3} - \sqrt{\overline{\mu}_1^2 + \overline{\mu}_2^2}|\,\|\mathbf{w}\|_2^2 \le 0. \tag{76}$$

Note that $\min(\varsigma_\phi^2/k_{v,1}, \varsigma_\alpha, \varsigma_\phi) - \max(\overline{k}_\rho, \overline{k}_\alpha + \overline{k}_\phi) > 0$ is obtained if the control gains $k_{v,1}$ and $k_{v,2}$ are chosen as $2\max(\overline{k}_\rho, \overline{k}_\alpha + \overline{k}_\phi) < 2k_{v,1} < k_{v,2}$. Now, if $k_{v,3}\|\mathbf{w}\|_2 < \varepsilon$, the following is obtained:

$$\dot{V} \le -|\min(\varsigma_\phi^2/k_{v,1}, \varsigma_\alpha, \varsigma_\phi) - \max(\overline{k}_\rho, \overline{k}_\alpha + \overline{k}_\phi)|(\rho^2 + \alpha'^2 + \phi^2) - k_{v,3}^2\|\mathbf{w}\|_2^2/\varepsilon + k_{v,3}\|\mathbf{w}\|_2. \tag{77}$$

The term $-k_{v,3}^2\|\mathbf{w}\|_2^2/\varepsilon + k_{v,3}\|\mathbf{w}\|_2$ attains its maximum value $\varepsilon/4$ at $k_{v,3}\|\mathbf{w}\|_2 = \varepsilon/2$. Then, (77) becomes

$$\dot{V} \le -|\min(\varsigma_\phi^2/k_{v,1}, \varsigma_\alpha, \varsigma_\phi) - \max(\overline{k}_\rho, \overline{k}_\alpha + \overline{k}_\phi)|(\rho^2 + \alpha'^2 + \phi^2) + \varepsilon/4. \tag{78}$$

Theorem 2. *Consider the system* (65)–(67) *with goal points in* Ω_{front}. *Let the control law be given by*

$$v_d = \sqrt{(k_{v,1}\rho\cos\alpha + v_1')^2 + l^2(k_{v,2}\sin\alpha - (k_{v,2} - k_{v,1}\cos\alpha)\phi + v_2')^2}, \tag{79}$$

$$\delta_d = -\arctan\left(l\left(\frac{k_{v,2}\sin\alpha - (k_{v,2} - k_{v,1}\cos\alpha)\phi + v_2'}{k_v\rho\cos\alpha + v_1'}\right)\right), \tag{80}$$

where v_1' *and* v_2' *are defined in* (74) and (75), *respectively, and* $\mathbf{w}$ *is given by*

$$\mathbf{w} = \begin{bmatrix} w_1 \\ w_2 \end{bmatrix} = \begin{bmatrix} (\varsigma_\phi/k_{v,1})(-\rho^2 + ((\sin\alpha - \phi)^2 - \phi^2)) + \sin\alpha(\sin\alpha - \phi) \\ (\varsigma_\phi/k_{v,1})(\sin\alpha - \phi) \end{bmatrix}. \tag{81}$$

Then, the solutions of (66)–(68) *are uniformly bounded around the origin.*

Proof. Let $(x_g, y_g) \in \Omega_{\text{front}}$. (78) is rewritten as

$$\dot{V} \le -|\min(\varsigma_\phi^2/k_{v,1}, \varsigma_\alpha, \varsigma_\phi) - \max(\overline{k}_\rho, \overline{k}_\alpha + \overline{k}_\phi)|\,(\rho^2 + (\sin\alpha - \phi)^2 + \phi^2) + \varepsilon/4. \tag{82}$$

Therefore, if

$$\sqrt{\rho^2 + (\sin\alpha - \phi)^2 + \phi^2}$$

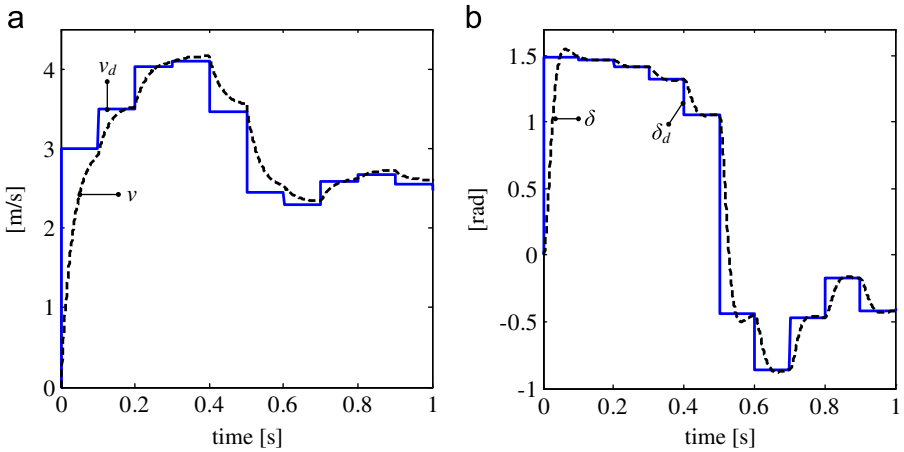

Fig. 5. Linear velocity and steering angle (simulation): (a) v_d (solid line) and v (dashed line) and (b) δ_d (solid line) and δ (dashed line).

$$\geq \sqrt{\varepsilon/(4|\min(\varsigma_\phi^2/k_{v,1},\varsigma_\alpha,\varsigma_\phi)-\max(\bar{k}_\rho,\bar{k}_\alpha+\bar{k}_\phi)|)},$$

$\dot{V} \leq 0$ is obtained. Then, $\rho(t)$, $\alpha(t)$, $\phi(t)$ are uniformly bounded around the origin (0, 0, 0). □

Corollary 2. *Consider the system* (65)–(67) *with goal points in* Ω_{rear}. *Let the control law be given by*

$$v_d = -\sqrt{(k_{v,1}\rho\cos\alpha+v_1')^2+l^2(k_{v,2}\sin\alpha+(k_{v,2}+k_{v,1}\cos\alpha)(\phi-\pi)-v_2')^2}, \tag{83}$$

$$\delta_d = -\arctan\left(l\left(\frac{k_{v,2}\sin\alpha+(k_{v,2}+k_{v,1}\cos\alpha)(\phi-\pi)-v_2'}{k_v\rho\cos\alpha+v_1'}\right)\right), \tag{84}$$

where v_1' *and* v_2' *are defined in* (74) and (75), *respectively, and* $\mathbf{w}$ *is given by*

$$\mathbf{w} = \begin{bmatrix} w_1 \\ w_2 \end{bmatrix} = \big[(\varsigma_\phi/k_{v,1})(-\rho^2+((-\sin\alpha-\phi+\pi)^2-(\phi-\pi)^2)) \\ -\sin\alpha(-\sin\alpha-\phi+\pi)(\varsigma_\phi/k_{v,1})(-\sin\alpha-\phi+\pi)\big]. \tag{85}$$

Then, the solutions of (65)–(67) *are uniformly bounded around* (0, π, π).

Proof. The proof is similar to Theorem 2. □

Remark 4. If $\rho = 0$, v_d and δ_d are chosen as in Remark 1.

$$v_d = k_{v,1}|\tilde{\theta}|, \tag{86}$$

$$\delta_d = -(\pi/2)\text{sgn}\tilde{\theta}. \tag{87}$$

In the presence of uncertainties, the position errors ($\tilde{x}$, $\tilde{y}$) cannot be guaranteed to stay at zero at all time. If, the control law (86) and (87) renders $(\tilde{x},\tilde{y}) \neq 0$, the control law switches to (79) and (80) if $(x_g,y_g) \in \Omega_{\text{front}}$ or (83) and (84) if $(x_g,y_g) \in \Omega_{\text{rear}}$.

4. Discrete-time analysis

The control laws in Section 3 were designed in the continuous-time domain. As discussed in Section 2.1, the measurement by NAV200 and the desired control inputs (v_d and δ_d) are updated every 100 ms. This becomes a sampled-data system. Let $T > 0$ be the sampling period. The control inputs $v_d(t)$ and $\delta_d(t)$ are held constants during the sampling interval $kT \leq t < (k+1)T$, $k = 0,1,2,\ldots$, and the navigation variables are updated at every sampling instance kT.

In Ω_{front}, the Euler-approximations of Eqs. (70)–(72) are

$$\rho(k+1) = \rho(k)-T((\varsigma_\phi^2/k_{v,1})\rho(k)+(\varsigma_\phi/k_{v,1})(v_1'+\mu_1)-\Delta_\rho), \tag{88}$$

$$\alpha'(k+1) = \alpha'(k)-T(\varsigma_\alpha\alpha'(k)-\varsigma_\phi\phi(k) \\ -((v_1'+\mu_1)/\rho)(\alpha'-\phi)(1+\varsigma_\phi/k_{v,1}) \\ -(\varsigma_\phi/k_{v,1})((v_2'+\mu_2)/l)-(\varsigma_\phi/k_{v,1})\Delta_\alpha-\Delta_\phi), \tag{89}$$

$$\phi(k+1) = \phi(k)-T(\varsigma_\phi\alpha'(k)+\varsigma_\phi\phi(k) \\ +((v_1'+\mu_1)/\rho)(\alpha'+\phi)-\Delta_\phi). \tag{90}$$

Here, the Lyapunov function $V(k) = \rho^2(k)+\alpha'^2(k)+\phi^2(k)$ is utilized. If $k_{v,3}\|\mathbf{w}\|_2 < \varepsilon$, the difference of V between time $k+1$ and k is given as

$$\Delta V = V(k+1)-V(k) \\ \leq T(-(\min(2\varsigma_\phi^2/k_{v,1}-Tk_{v,1},2\varsigma_\alpha-T(\varsigma_\alpha+\varsigma_\phi^2/k_{v,1}),2\varsigma_\phi-T\varsigma_\phi^2) \\ -\max(\bar{k}_\rho,\bar{k}_\alpha+\bar{k}_\phi))(\rho^2+\alpha'^2+\phi^2)+\varepsilon/2). \tag{91}$$

Let

$$\eta = \min(2\varsigma_\phi^2/k_{v,1}-Tk_{v,1},2\varsigma_\alpha \\ -T(\varsigma_\alpha+\varsigma_\phi^2/k_{v,1}),2\varsigma_\phi-T\varsigma_\phi^2)-\max(\bar{k}_\rho,\bar{k}_\alpha+\bar{k}_\phi).$$

Note that $\eta > 0$ if the control gains $k_{v,1}$ and $k_{v,2}$ are chosen as $2\max(\bar{k}_\rho,\bar{k}_\alpha+\bar{k}_\phi) < 2k_{v,1} < k_{v,2} < 1/T$. Then, if $\sqrt{\rho^2+(\sin\alpha-\phi)^2+\phi^2} \geq \sqrt{\varepsilon/2\eta}$, $\Delta V \leq 0$ is obtained. Therefore, using the control law (79) and (80) for $(x_g,y_g) \in \Omega_{\text{front}}$, $\rho(k)$, $\alpha(k)$, and $\phi(k)$ become uniformly bounded around the origin (0, 0, 0). Using the same procedure as in (91) for $(x_g,y_g) \in \Omega_{\text{rear}}$, the discrete time analysis of the control law (83) and (84) yields the same result, that is, $\rho(k)$, $\alpha(k)$, and $\phi(k)$ are uniformly bounded around (0, π, π).

5. Simulation and experimental results

5.1. Simulation results

In this section, the performance of the proposed control laws is illustrated through simulations. The forklift mass is $m = 1500$ kg. The mass moment of inertia of the vehicle with respect to O_b is set to $I_b = 350$ kg m^2 and that of the rear wheel around the normal axis is $I_\delta = 1.2$ kg m^2. The mass moments of inertia of the front and

rear wheels around their individual rolling axes are $I_f=0.1$ kg m^2 and $I_r=0.6$ kg m^2, respectively. The radii of the front and rear wheels are $r_f=25$ mm and $r_r=150$ mm, respectively. The motor parameters are set to $k_{m,v}=k_{m,\delta}=87.7$ N m/A, $k_{m,v}=k_{m,\delta}=0.75\,\Omega$, and $k_{emf,v}=k_{emf,\delta}=0.6$ V s/rad. The surface frictions in the directions of v and δ are modeled as follows (Lee & Kim, 1995):

$$f_v=(f_v^C-\Delta f_v^C(1-\exp(-v/v_S))+f_v^c v/r_r)\mathrm{sgn}(v), \tag{92}$$

$$f_\delta=(f_\delta^C-\Delta f_\delta^C(1-\exp(-\dot\delta/\dot\delta_S))+f_\delta^c\dot\delta)\mathrm{sgn}(\dot\delta), \tag{93}$$

where $f_v^C-\Delta f_v^C$ and $f_\delta^C-\Delta f_\delta^C$ are the Coulomb frictions, $\Delta f_v^C\exp(-v/v_S)$ and $\Delta f_\delta^C\exp(-\dot\delta/\dot\delta_S)$ are the Stribeck effects (v_S and $\dot\delta_S$ are the critical Stribeck velocities), and f_v^c and f_δ^c are the viscous frictions. The friction parameters are set to $f_v^C=f_\delta^C=1.2$ N, $\Delta f_v^C=\Delta f_\delta^C=1.0$ N, $v_S=0.1$ m/s, $\dot\delta_S=0.2$ rad/s, $f_v^c=f_\delta^c=0.5$ N s. The modeling errors are considered as the slip-angle at point O_b during motion as $-0.1\mathrm{sgn}(\dot\theta)$. The measurement noises were given as random signals with bounds $\bar n_x=\bar n_y=0.01$ m and $\bar n_\theta=0.001$ rad. The PD control gains of the driving and steering motors are set to $k_{P,v}$, $k_{P,\delta}=400$ Vs/m 50 V/rad, $k_{D,v}=0.1$ Vs^2/m, $k_{D,\delta}=1$ Vs/rad. Fig. 5(a) and (b) illustrates the difference between the desired commands generated from the outer loop (v_d and δ_d) with those in the inner loop (v and δ), which are through the PD control of the AC motors (simulation result).

To compare the performance of the two control laws (with and without the consideration of uncertainties), a backward navigation from an initial configuration $(x, y, \theta)=(3, 3, 0)$ to a goal configuration $(x, y, \theta)=(0, 0, 0)$ is simulated. The units of x and y are in meters and that of θ is radian. The gains are set to $k_{v,1}=0.5$ s^{-1}, $k_{v,2}=5$ s^{-1}, $k_{v,3}=0.2$ s^{-1}, and $\varepsilon=0.005$ s^{-1}. The trajectories of the forklift to the goal configuration are shown in Fig. 6. The motions of the forklift in time, $(x(t), y(t), \theta(t))$, under two different control laws, (54) and (55) vs. (83) and (84), are compared in Fig. 7. With the control law (54) and (55), the forklift arrived at (0.110, −0.010, 0.012) at $t=8$ s, while using (83) and (84), it reached (0.013, −0.010, 0.000). A faster convergence was achieved with (83) and (84). Figs. 8 and 9 compare the applied control commands v_d and δ_d, respectively, during this navigation.

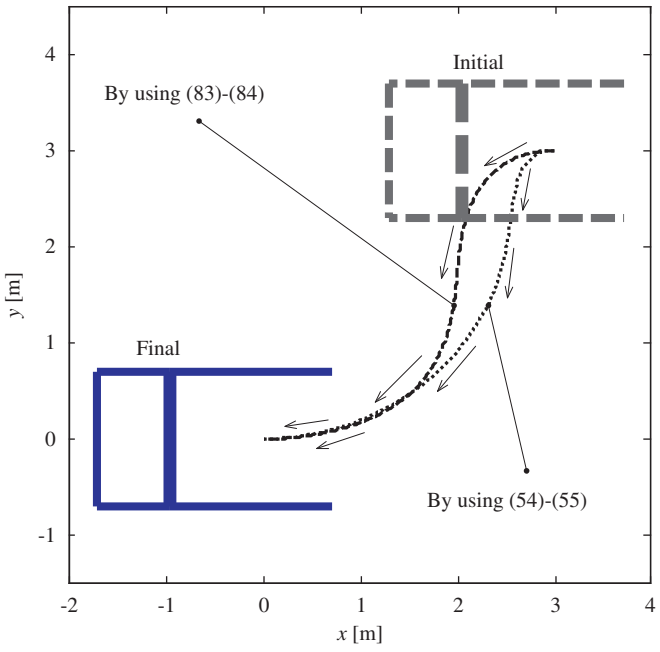

Fig. 6. Comparison of configuration control with and without the consideration of uncertainties (simulation).

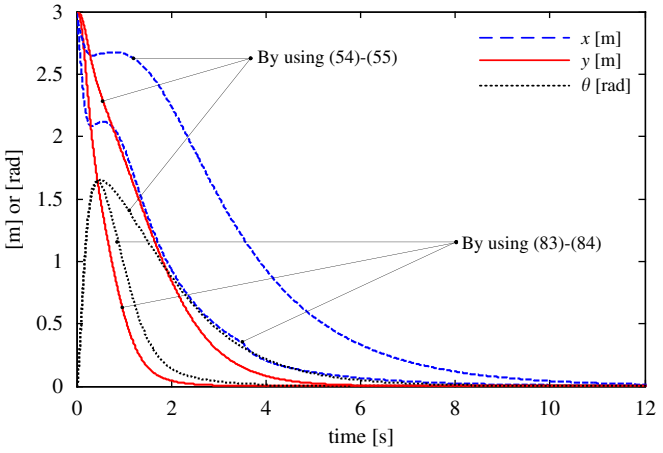

Fig. 7. Comparison of motions of the forklift under two different control laws: a faster approach was achieved with the control law considering uncertainties (simulation).

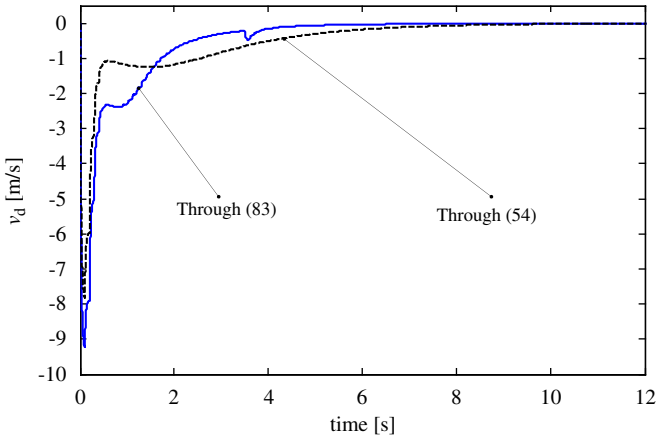

Fig. 8. Linear velocities in Fig. 6: through (83) (solid line) vs. through (54) (dashed line).

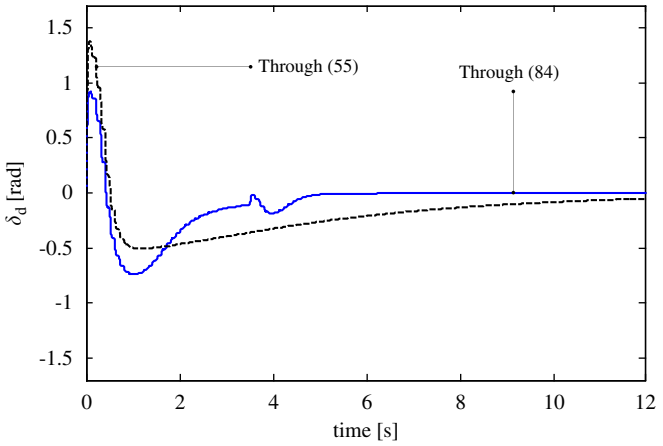

Fig. 9. Steering angles in Fig. 6: through (84) (solid line) vs. through (55) (dashed line).

Now, consider the typical situation that the forklift has already reached the goal point but the orientation error is still huge. Assume that $\rho=0$ and $\tilde\theta=-\pi/2$. Which is the case that the vehicle is steered from $(0, 0, \pi/2)$ to $(0, 0, 0)$, see Fig. 10. The gains are set to the same values as in the previous simulation. Also the same uncertainties are assumed. As seen in Fig. 10, the vehicle has

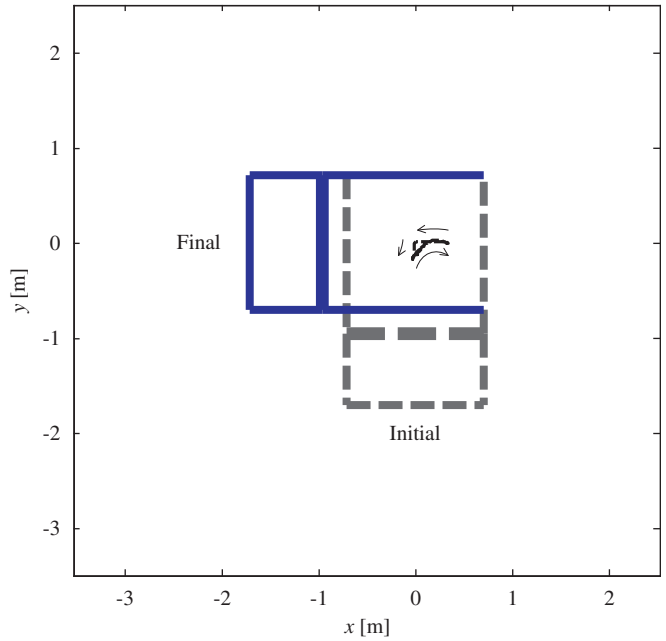

Fig. 10. Orientation control when the position error is zero but the orientation error is $-\pi/2$ (simulation): the vehicle moves back and forth several times to make the orientation error zero: (79) and (80) are used in Ω_{front} and (83) and (84) are used in Ω_{rear}.

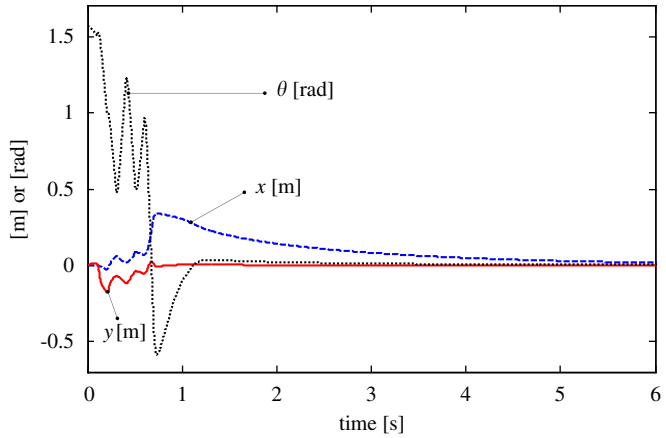

Fig. 11. Motions of the forklift when achieving a pure orientation control ($\rho=0$ and $\tilde{\theta}=-\pi/2$) in Fig. 10.

to move back and forth several times to achieve the desired orientation in this case. The detailed motions of the forklift in time are shown in Fig. 11. Figs. 12 and 13, respectively, depict the control commands v_{d} and δ_{d} in achieving the orientation control in Fig. 10. The position and orientation values of the forklift at $t=6$ s was (0.010, 0.000, 0.002), which is quite acceptable.

6. Experimental results

In this subsection, two experimental results are presented. The first experiment evaluates the control law (79) and (80) in steering the forklift forward from the initial configuration $(-5.55,\ 1.58,\ -0.71)$ to the goal configuration (0, 0, 0), while the second experiment tests the control law (83) and (84) in steering it backward from $(4.75,\ -1.3,\ -0.16)$ to (0, 0, 0). The gains were $k_{v,1}=0.3\ \text{s}^{-1}$, $k_{v,2}=5\ \text{s}^{-1}$, $k_{v,3}=0.2\ \text{s}^{-1}$, and $\varepsilon=0.01\ \text{s}^{-1}$. Figs. 14–17 depict the trajectories in the x–y plane, the vehicle motions, the

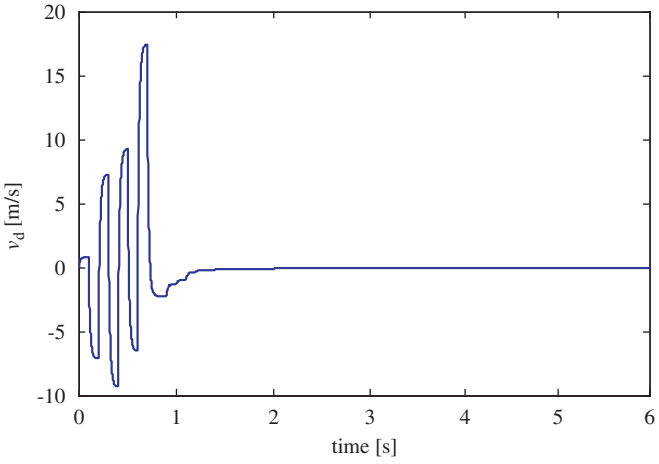

Fig. 12. Applied v_{d} in Fig. 10.

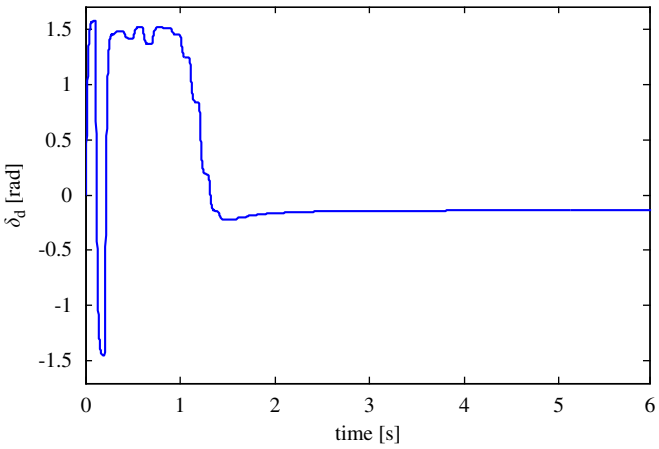

Fig. 13. Applied δ_{d} in Fig. 10.

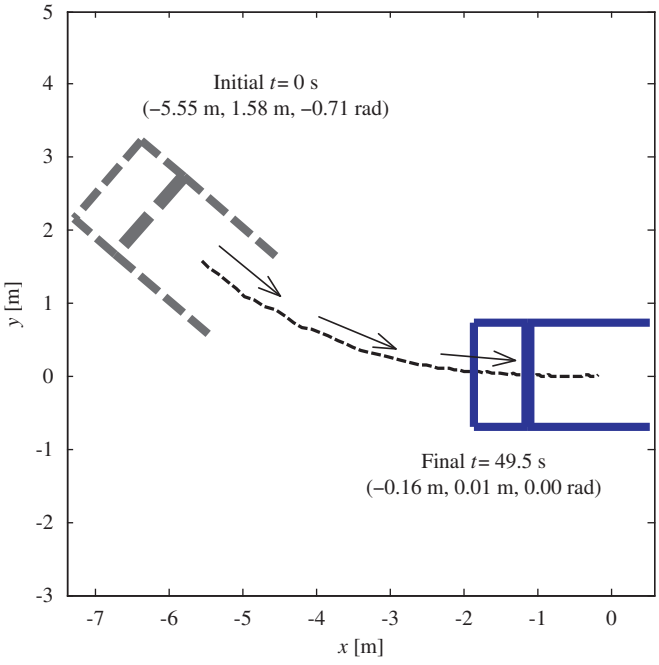

Fig. 14. Trajectories of the forklift in reaching the target configuration in forward movement using the control law (79) and (80) (experiment).

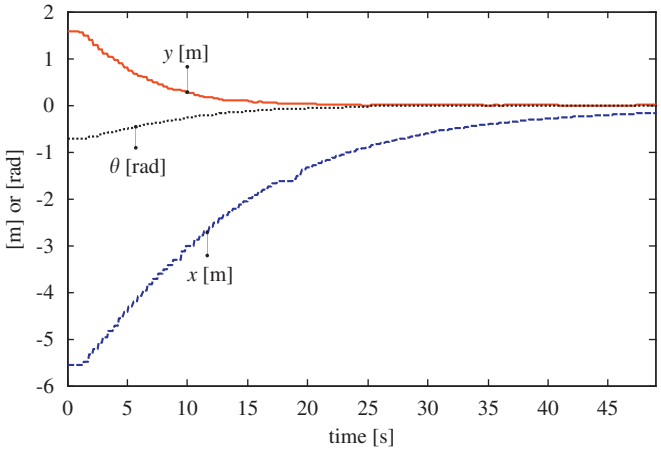

Fig. 15. The forklift motions in time of Fig. 14.

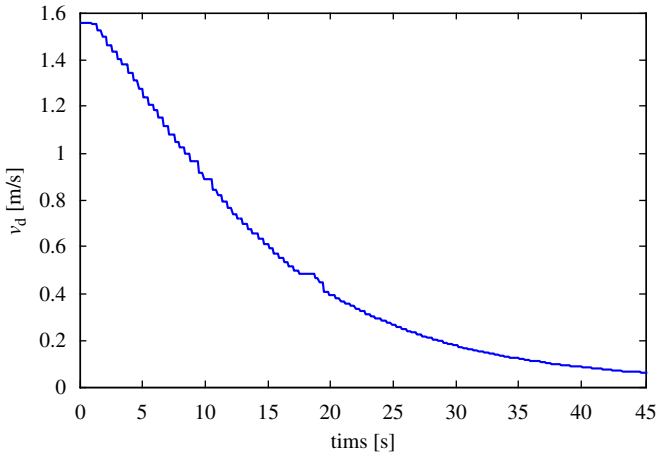

Fig. 16. Linear velocity command v_d of Fig. 14.

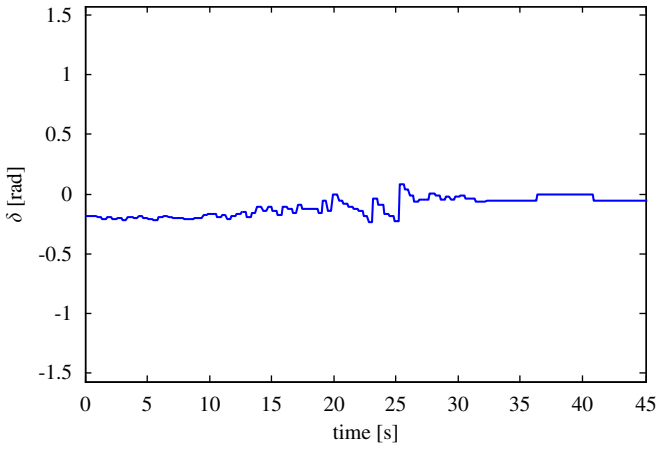

Fig. 17. Steering angle command δ_d of Fig. 14.

linear velocity command, and the steering angle command, respectively, of the forward movement, and Figs. 18–21 show those of the backward movement. For the forward movement, the forklift stopped at $x=-0.16$ m, $y=0.01$ m, and $\theta=0.00$ rad at 49.5 s, while for the backward movement, it stopped at $x=0.20$ m, $y=0.01$ m, and $\theta=-0.02$ rad at 35 s.

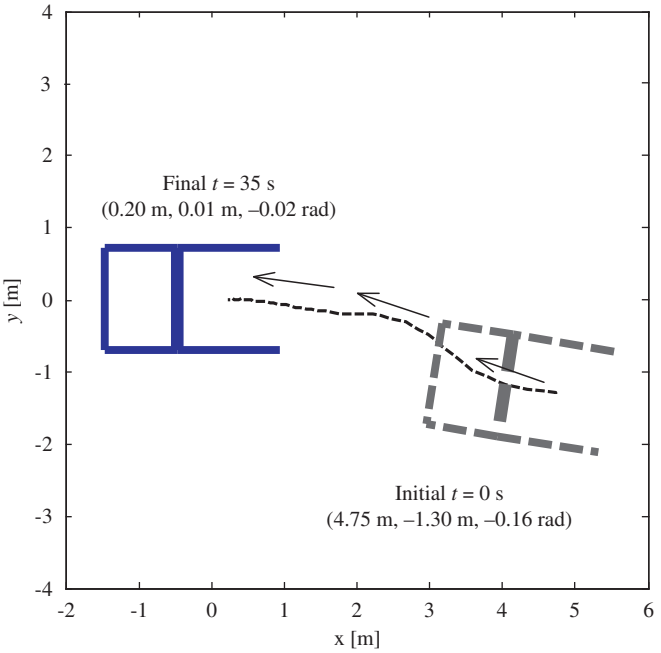

Fig. 18. Trajectories of the vehicle in reaching the target configuration in backward movement using (83) and (84) (experiment).

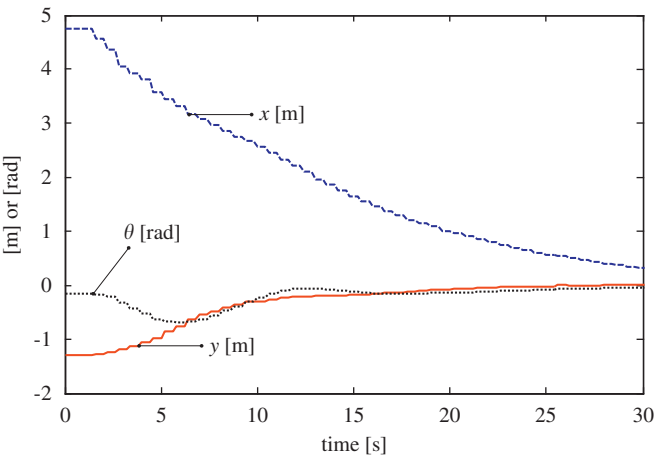

Fig. 19. The forklift motions in time of Fig. 18.

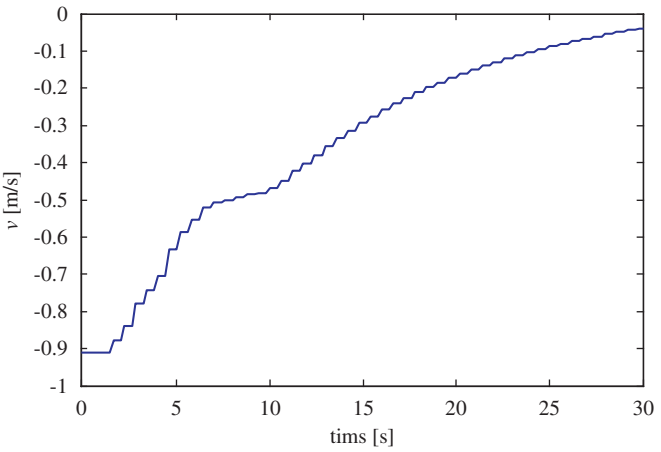

Fig. 20. Linear velocity command v_d of Fig. 18.

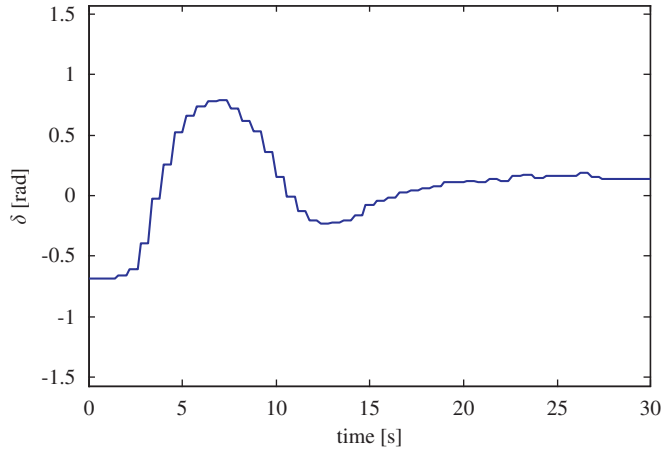

Fig. 21. Steering angle command δ_d of Fig. 18.

7. Conclusions

In this paper, a robust configuration control of a forklift was developed. A two-loop (outer and inner) control for automating forklifts was adopted. Since the forward motion and backward motion of the forklift were not symmetric, two different control laws for individual motions were designed. For a nominal model that does not involve any uncertainty (no slip and no noise), the uniform asymptotic stability of the desired configuration was achieved. However, in the presence of modeling uncertainty and measurement noises, the developed control law assured the uniform boundedness. The discrete-time analysis of the proposed control law was performed. The range of control gains in regard to the sampling period was clarified. Both simulation and experimental results showed that the proposed method is robust against uncertainties in obtaining fast and natural trajectories.

Acknowledgment

This work was supported by the Regional Research Universities Program (Research Center for Logistics Information Technology, LIT) and the World Class University (grant no. R31-20004) granted by the National Research Foundation of Korea under the Ministry of Education, Science and Technology, Korea.

Appendix A. Supporting information

Supplementary data associated with this article can be found in the online version at doi:10.1016/j.conengprac.2011.11.007.

References

Aicardi, M., Casalino, G., Bicchi, A., & Balestrino, A. (1995). Closed loop steering of unicycle-like vehicles via Lyapunov techniques. *IEEE Robotics and Automation Magazine*, *2*(1), 27–35.

Ailon, A., Berman, N., & Arogeti, S. (2005). On controllability and trajectory tracking of a kinematic vehicle model. *Automatica*, *41*(5), 889–896.

Astolfi, A. (1996). Discontinuous control of nonholonomic systems. *Systems & Control Letters*, *27*(1), 37–45.

Brockett, R. W. (1983). Asymptotic stability and feedback stabilization. In: R. W. Brockett, R. S. Millman, & H. J. Sussmann (Eds.), *Differential geometric control theory* (pp. 181–191). Boston: Birkhauser.

Buccieri, D., Perritaz, D., Mullhaupt, P., Jiang, Z.-P., & Bonvin, D. (2009). Velocity-scheduling control for a unicycle mobile robot: theory and experiments. *IEEE Transactions on Robotics*, *25*(2), 451–458.

Bui, T. T. Q., & Hong, K.-S. (2010). Sonar-based obstacle avoidance using region partition scheme. *Journal of Mechanical Science and Technology*, *24*(1), 365–372.

Corradini, M. L., & Orlando, G. (2002). Control of mobile robots with uncertainties in the dynamic model: a discrete time sliding mode approach with experimental results. *Control Engineering Practice*, *10*(1), 23–24.

De La Cruz, C., Bastos, T. F., & Carelli, R. (2011). Adaptive motion control law of a robotic wheelchair. *Control Engineering Practice*, *19*(2), 113–125.

Fierro, R., & Lewis, F. L. (1998). Control of a nonholonomic mobile robot using neural networks. *IEEE Transactions on Neural Networks*, *9*(4), 589–600.

Floquet, T., Barbot, J.-P., & Peruquetti, W. (2003). Higher-order sliding mode stabilization for a class of nonholonomic perturbed systems. *Automatica*, *39*(6), 1077–1083.

Ge, S. S., Wang, Z., & Lee, T. H. (2003). Adaptive stabilization of uncertain nonholonomic systems by state and output feedback. *Automatica*, *39*(8), 1451–1460.

Hespanha, J. P., & Morse, A. S. (1999). Stabilization of nonholonomic integrators via logic-based switching. *Automatica*, *35*(3), 385–393.

Hong, K.-S., Tamba, T. A., & Song, J. B. (2008). Mobile robot architecture for reflexive avoidance of moving obstacles. *Advanced Robotics*, *22*(13–14), 1397–1420.

Jiang, Z. P. (2000). Robust exponential regulation of nonholonomic systems with uncertainties. *Automatica*, *36*(2), 189–209.

Khalil, H. K. (2002). *Nonlinear control systems* (3rd ed.). New Jersey: Prentice-Hall.

Lee, S.-W., & Kim, J.-H. (1995). Robust adaptive stick-slip friction compensation. *IEEE Transactions on Industrial Electronics*, *42*(5), 474–479.

Lin, W.-S., & Yang, P.-C. (2008). Adaptive critic motion control design of autonomous wheeled mobile robot by dual heuristic programming. *Automatica*, *44*(11), 2716–2723.

Lucibello, P., & Oriolo, G. (2001). Robust stabilization via iterative state steering with an application to chained form systems. *Automatica*, *37*(1), 71–79.

Marchand, N., & Alamir, M. (2003). Discontinuous exponential stabilization of chained form systems. *Automatica*, *39*(2), 343–348.

Martins, N. F., Celeste, W. C., Carelli, R., Sarcinelli-Filho, M., & Bastos-Filho, T. F. (2008). An adaptive dynamic controller for autonomous mobile robot trajectory tracking. *Control Engineering Practice*, *16*(11), 1354–1363.

Morin, P., & Samson, C. (2009). Control of nonholonomic mobile robots based on the transverse function approach. *IEEE Transactions on Robotics*, *25*(5), 1058–1073.

Moustris, G. P., & Tzafestas, S. G. (2011). Switching fuzzy tracking control for mobile robots under curvature constraints. *Control Engineering Practice*, *19*(1), 45–53.

Murray, R. M., & Sastry, S. S. (1993). Nonholonomic motion planning: Steering using sinusoids. *IEEE Transactions on Automatic Control*, *38*(5), 700–716.

Oriolo, G., De Luca, A., & Vendittelli, M. (2002). WMR control via dynamic feedback linearization: Design, implementation, and experimental validation. *IEEE Transactions on Control Systems Technology*, *10*(6), 835–852.

Park, B. S., Yoo, S. J., Park, J. B., & Choi, Y. H. (2009). Adaptive neural sliding mode control of nonholonomic wheeled mobile robots with model uncertainty. *IEEE Transactions on Control Systems Technology*, *17*(1), 207–214.

Prieur, C., & Astolfi, A. (2003). Robust stabilization of chained systems of hybrid control. *IEEE Transactions on Automatic Control*, *48*(10), 1768–1772.

Ryu, J.-C., & Agrawal, S. K. (2010). Planning and control of under-actuated mobile manipulators using differential flatness. *Autonomous Robot*, *29*(1), 35–52.

Rossomando, F. G., Soria, C., & Carelli, R. (2011). Autonomous mobile robots navigation using RBF neural compensator. *Control Engineering Practice*, *19*(3), 215–222.

Samson, C. (1995). Control of chained systems application to path following and time-varying point stabilization of mobile robots. *IEEE Transactions on Automatic Control*, *40*(1), 64–77.

Scaglia, G., Rosales, A., Quintero, L., Mut, V., & Agarwal, R. (2010). A linear-interpolation-based controller design for trajectory tracking of mobile robots. *Control Engineering Practice*, *18*(3), 318–329.

Shim, H.-S., & Sung, Y.-G. (2004). Stability and four-posture control for nonholonomic mobile robots. *IEEE Transactions on Robotics*, *20*(1), 148–154.

Siegwart, R., & Nourbakhsh, I. R. (2004). *Introduction to autonomous mobile robot*. Cambridge, MA: MIT Press.

Tamba, T. A., Hong, B., & Hong, K.-S. (2009). A path following control of an unmanned autonomous forklift. *International Journal of Control, Automation, and Systems*, *7*(1), 113–122.

Tang, C.P., Miller, P.T., Krovi, V.N., Ryu, J.-C., & Agrawal, S.K. (2008). Kinematic control of a nonholonomic wheeled mobile manipulator–a differential flatness approach. In *Proceedings of the ASME Dynamic Systems and Control Conference.* DSCC2008-2253, Ann Harbor, Michigan, USA.

Treesatayapun, C. (2011). A discrete-time stable controller for an omni-directional mobile robot based on approximated model. *Control Engineering Practice*, *19*(2), 194–203.

Widyotriatmo, A., Hong, B., & Hong, K.-S. (2009). Predictive navigation of an autonomous vehicle with nonholonomic and minimum turning radius constraints. *Journal of Mechanical Science and Technology*, *23*(2), 381–388.

Widyotriatmo, A., Hong, K.-S., & Prayudhi, L. H. (2010). Robust stabilization of a wheeled vehicle: Hybrid feedback control design and experimental validation. *Journal of Mechanical Science and Technology*, *24*(2), 513–520.

Widyotriatmo, A., & Hong, K.-S. (2011). Navigation function-based control of multiple wheeled vehicles. *IEEE Transactions on Industrial Electronics*, *58*(5), 1896–1906.

Xi, Z., Feng, G., Jiang, Z. P., & Cheng, D. (2003). A switching algorithm for global exponential stabilization of uncertain chained systems. *IEEE Transactions on Automatic Control*, *48*(10), 1793–1798.

Yoon, Y., Shin, J., Kim, H. J., Park, Y., & Sastry, S. S. (2009). Model-predictive active steering and obstacle avoidance for autonomous ground vehicles. *Control Engineering Practice*, *17*(7), 741–750.